Research Article | Vol. 27, No. 15 | 22 Jul 2019 | OPTICS EXPRESS 20745
Optics EXPRESS

Influence of pump coherence on the generation of position-momentum entanglement in optical parametric down-conversion

WUHONG ZHANG,[1,2] ROBERT FICKLER,[2,3] ENNO GIESE,[2,4,6] LIXIANG CHEN,[1,7] AND ROBERT W. BOYD[2,5]

[1]*Department of Physics, Jiujiang Research Institute and Collaborative Innovation Center for Optoelectronic Semiconductors and Efficient Devices, Xiamen University, Xiamen 361005, China*
[2]*Department of Physics, University of Ottawa, 25 Templeton Street, Ottawa, Ontario K1N 6N5, Canada*
[3]*current address: Photonics Laboratory, Physics Unit, Tampere University, Tampere, FI-33720, Finland*
[4]*current address: Institut für Quantenphysik and Center for Integrated Quantum Science and Technology (IQ^{ST}), Universität Ulm, Albert-Einstein-Allee 11, D-89081, Germany*
[5]*Institute of Optics, University of Rochester, Rochester, NY 14627, USA*
[6]*enno.a.giese@gmail.com*
[7]*chenlx@xmu.edu.cn*

Abstract: We examine experimentally how the degree of position-momentum entanglement of photon pairs depends on the transverse coherence of the pump beam that excites them in a process of spontaneous parametric down-conversion. Using spatially incoherent light from a light-emitting diode, we obtain strong position correlation of the photons, but we find that transverse momentum correlation, and thus entanglement, is entirely absent. When we continuously vary the degree of spatial coherence on the pump beam, we observe the emergence of stronger momentum correlations and entanglement. We present theoretical arguments that explain our experimental results. Our results shed light on entanglement generation and can be applied to control entanglement for quantum information applications.

1. Introduction

Strong correlations in two conjugate variables are *the* signature of quantum entanglement and have played a key role in the development of modern physics [1, 2]. Entangled photons have become a standard tool in quantum information [3] and foundations [4, 5]. They have been explored to generate nonclassical correlations among different degrees of freedom, such as polarization [4–6], time and frequency [7–9], position and momentum [10] as well as angular position and orbital angular momentum [11, 12]. Entanglement of two-dimensional systems, in analogy to classical bits, is *the* primary resource for quantum communication and processing [3]. In addition, multiple-level quantum systems can show high-dimensional entanglement with a high complexity [13–15] and can be exploited for various quantum information tasks [16]. Position-momentum entanglement [10] as a continuous degree of freedom is the ultimate limit of high-dimensional entanglement and its deeper understanding is essential for the development of novel quantum technologies.

Position-momentum-entangled photon pairs can be rather straight-forwardly generated in spontaneous parametric down-conversion (SPDC) [10, 17], the workhorse of many quantum optics labs. In this process, a strong pump beam spontaneously generates a pair of signal and idler photons through a nonlinear interaction. Formation of position-momentum entanglement is often explained by simple heuristic arguments: A pump photon is converted at one particular transverse position into signal and idler photons. If we denote the transverse positions by x_s and x_i, respectively, the distance $x_- \equiv (x_s - x_i)/\sqrt{2}$ between the two photons vanishes because of their common birth place. Hence, the photons are correlated and the uncertainty Δx_-^2 is vanishingly

#368244 https://doi.org/10.1364/OE.27.020745
Journal © 2019 Received 11 Jun 2019; accepted 12 Jun 2019; published 10 Jul 2019

Optics EXPRESS

small. In addition, transverse momentum conservation requires the generated photons to travel in opposite directions, so that the average momentum $p_+ \equiv (p_s + p_i)/\sqrt{2}$ vanishes. Here, p_s and p_i denote the transverse momenta of signal and idler photons, respectively. They are anti-correlated so that the uncertainty Δp_+^2 is vanishingly small. Hence, it is possible that the product of the uncertainties *violates* the inequality

$$\Delta x_-^2 \Delta p_+^2 \geq \hbar^2/4, \tag{1}$$

which is based on the Heisenberg uncertainty relations of conjugate variables for separable systems. A violation of this inequality is a witness for position-momentum entanglement [2]. Thus, the strong position and momentum correlations as implied by the common birth zone of signal and idler photons [18] together with momentum conservation are the key signature of entanglement. However, these arguments have not taken the coherence properties of the pump beam, i.e. the quantum aspect of the driving force behind the pair generation, into account. The influence of different pump shapes on entanglement and on the propagation of the generated pairs have been explored [19–23]. The impact of the temporal coherence of the pump has also been investigated in [24–26] and the transfer of the spatial pump coherence to the down-converted light was theoretically studied in [27, 28].

In this article, we study how the generation of position-momentum entangled photon pairs relies on the coherence properties of the pump. For that, we pump a nonlinear crystal by a coherent light source (a laser), a *true* incoherent source (an LED), and examine the transition between these extreme cases by pumping with pseudo-thermal light of variable partial coherence. We find that the strength of the momentum anti-correlation depends strongly on the coherence of the pump so that the degree of entanglement can be adjusted. Fundamentally, our analysis demonstrates that the lack of momentum correlation does not imply an violation of the conservation of momenta; it shows that the coherence of the pump, i.e. its 'quantumness', is crucial for the generation of entangled photons.

2. Experimental setup

In our experiment shown in Fig. 1, the coherent pump source is a laser diode module (Roithner LaserTechnik, RLDE405M-20-5), which can be turned into a pseudo-thermal light source by modulating the transverse phase profile with a spatial light modulator (SLM, Hamamatsu X10468-05). The SLM is either used as a simple mirror or to generate a pseudo-thermal light source with varying transverse coherence [29] and a beam waist of $w = 0.11$ mm in the crystal. The incoherent source is a blue LED [30, 31] with a center wavelength of 405 nm and an output power of up to 980 mW (Thorlabs M405L3). To ensure a Gaussian-like beam profile while maintaining transverse incoherence, we couple the light into a 400-µm-core multimode fiber. The out-coupled LED beam is then demagnified by a $4f$-system before it enters the crystal. To ensure the same polarization for both sources, we introduce polarizers in both beam paths. We add a 3-nm-bandpass filter at 405 nm in front of the crystal to reduce the broad spectrum of the LED. After this filtering, we measure a pump power of 20 µW for the laser and 130 µW for the LED at the crystal.

In all pump scenarios, the photon pairs are generated by a 1 mm×2 mm×5 mm periodically poled potassium titanyl phosphate (ppKTP) crystal, which is phase-matched for type-II collinear emission. A long-pass filter and a 3-nm-spectral filter at 810 nm after the crystal block the pump beam and ensure that only frequency-degenerate photons are detected. We split the photon pairs into two separate paths by means of a polarizing beam splitter. In each path we place a narrow vertical slit of about 100 µm width, which can be translated in the horizontal direction and detects either position or momentum depending on the optical system (see below). Photons passing through the vertical slits are collected by microscope objectives, coupled into multimode fibers, and detected by avalanche photodiode single-photon counting modules. The photon coincidence

Optics EXPRESS

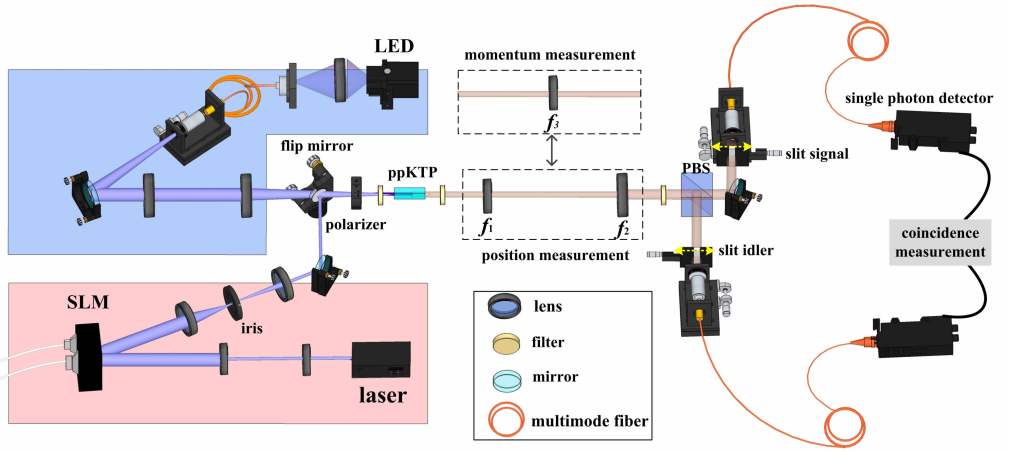

Fig. 1. Schematic of the experimental setup. Photon pairs are generated by pumping a type-II nonlinear crystal (ppKTP) with either a laser beam with adjustable transverse coherence (red shaded beam path) or a beam derived from an LED that is spatially incoherent (blue shaded beam path). The coherence of the laser is tuned by modulating the transverse phase profile with a spatial light modulator (SLM). A polarizing beam splitter (PBS) splits the pairs and their joint spatial distributions are measured by independently movable slits in each arm. They are followed by bucket detector systems consisting of microscope objectives, multimode fibers, single-photon detectors. Position correlations are registered by a coincidence measurement in the image plane (f_1 and f_2), while momentum correlations are observed in the focal plane of a lens f_3 (Fourier transform plane, or momentum space).

count rate is recorded with a coincidence window of 1 ns and as a function of the two distances d_s and d_i of the slits from the optical axis. To measure the joint position distribution, we image the exit face of the crystal onto the planes of the slits with a $4f$-system consisting of two lenses with focal lengths $f_1 = 50\,\text{mm}$ and $f_2 = 150\,\text{mm}$ (placed prior to the beam splitter). We magnify the down-converted beam to reduce errors that arise from the finite precision of the slit widths. By replacing the $4f$-system with a single lens f_3 and placing the two slits in the Fourier planes of the lens, we measure correlations of the transverse momenta of the photons. We use a focal length of $f_3 = 100\,\text{mm}$ for the laser and a shorter focal length of $f_3 = 50\,\text{mm}$ for the LED to account for the broader momentum distribution of the LED beam. Again, we record the coincidence count rate as a function of the position of each slit, and we transform the distance $d_{s,i}$ to momentum through the relation $p_{s,i} \cong \hbar d_{s,i} k_{s,i}/f_3$. Here, $k_{s,i}$ denotes the wave number of the signal or idler field.

To generate a Gaussian Schell model beam, we imprint with the SLM different random phase patterns on the pump laser. The statistics of these random patterns is Gaussian with a transverse width in the crystal of $\delta_\phi = 0.11\,\text{mm}$. To tune the coherence length, we vary the strength of the modulation ϕ_0 and obtain the coherence length from $l_c = \delta_\phi/\phi_0$ [29]. For each modulation strength, we display around 300 different patterns, average over the observed counts per measurement setting, and evaluate the obtained uncertainties Δx_-^2 and Δp_+^2.

3. Laser- versus LED-generated correlations

As a first experimental test we investigate position-momentum entanglement for the two extreme cases of the pump, a perfectly coherent laser and a truly incoherent LED light source. The setup described above (see Fig. 1) is designed in a flexible manner so that switching between the laser and the LED (red and blue shaded regions in Fig. 1) can be easily accomplished with a flip mirror. We can further change between detecting position and momentum correlations simply by using a

Optics EXPRESS

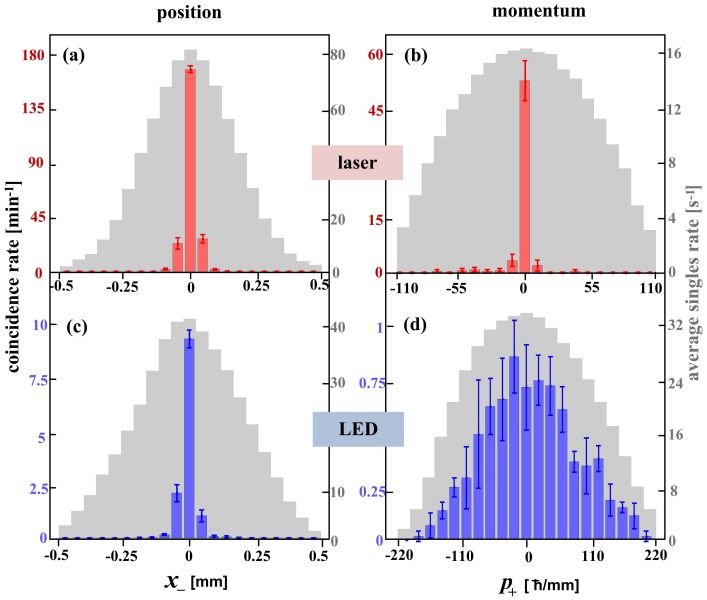

Fig. 2. Position correlations and momentum anti-correlations of SPDC pumped by a laser and an LED. We obtain the coincidence rates in (a,c) by moving the two slits in opposite directions in the near field (measuring the distribution of x_-) and in (b,c) by moving them in the same directions in the far field (measuring the distribution of p_+). The acquisition time of each data point is 1 min for the laser pump (a,b) and 15 min for the LED pump (c,d); the error bars are obtained by averaging over five such measurements. To demonstrate the correlation strength graphically, we show the average rate of singles counts (gray distributions in the back; scale on the right side of each plot).

different set of lenses. To investigate entanglement, we measure the probability distributions of the distance x_- between signal (s) and idler (i) photons, as well as their average momentum p_+ and compare the results obtained for both sources.

The distributions of x_- for both sources are shown in Fig. 2(a) and (c). The positions of signal and idler photons are highly correlated and the shapes of the two distributions coincide, underlining argument of a common birth zone. For the momenta, the distributions of p_+ obtained with a laser and with an LED differ significantly, see Fig. 2(b) and (d). The momenta of the photons generated by the laser are anti-correlated, in agreement with the argument of momentum conservation. We further verify entanglement, since the measured uncertainty product

$$\Delta x_-^2 \Delta p_+^2\big|_{\text{laser}} = (0.0112 \pm 0.0005)\hbar^2 \tag{2}$$

violates inequality (1). Here, as well as in all following discussions, we obtain the uncertainties by a Gaussian fit to the experimental data. In contrast, the momenta obtained from an LED-pumped source are uncorrelated, and the broad distribution leads to

$$\Delta x_-^2 \Delta p_+^2\big|_{\text{LED}} = (4.62 \pm 0.93)\hbar^2, \tag{3}$$

consistent with inequality (1), implying that entanglement is not present and seemingly in contrast to the argument of momentum conservation.

4. Joint probability distributions

For a more detailed analysis, we measure the entire joint probability distributions for position space $\mathcal{P}(x_s, x_i)$ and momentum space $P(p_s, p_i)$ for both the laser and the LED. The joint

Optics EXPRESS

momentum distribution $P(p_s, p_i) = P_{\mathcal{E}} P_{\chi}$ in a spontaneous parametric down-conversion process consists two parts: (i) the angular profile of the pump $P_{\mathcal{E}} \propto |\mathcal{E}(p_s + p_i)|^2$, where $\mathcal{E}$ is the angular field amplitude, and (ii) the phase-matching function P_{χ}, which depends on the the mismatch $\Delta\kappa \equiv \kappa_p - \kappa_s - \kappa_i$. Here, $\kappa_{p,s,i}$ are the longitudinal components of the wave vectors of the pump, signal, and idler fields. For a bulk crystal of length L, the phase-matching function takes the familiar form $P_{\chi} \propto \mathrm{sinc}^2(\Delta\kappa L/2)$, but for other configurations it depends on the crystal poling and other properties that arise from the propagation of the light through the medium. If we assume a crystal of infinite transverse size, we obtain precise transverse momentum conservation, as is apparent from the argument $p_s + p_i$ of $\mathcal{E}$.

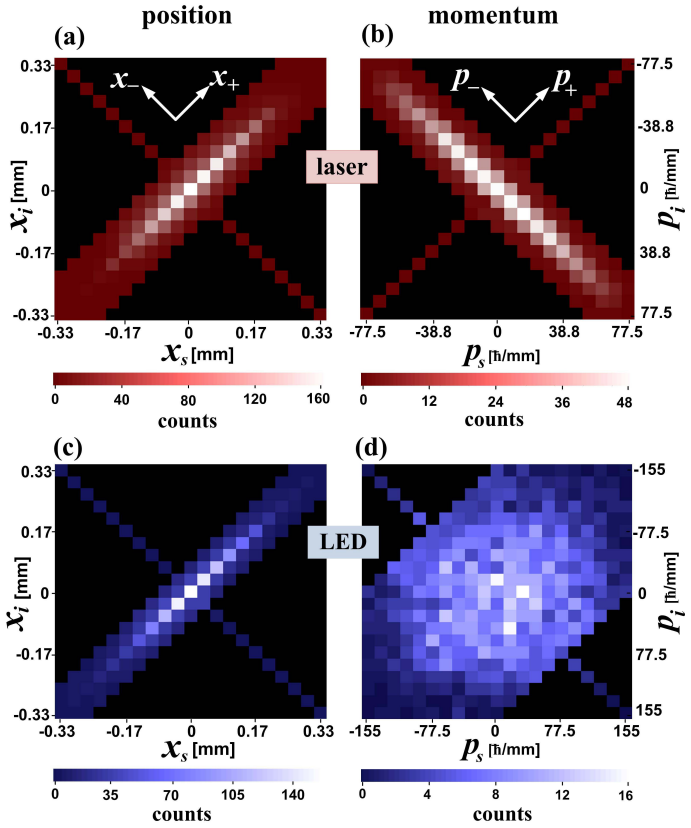

Fig. 3. Effect of coherence on joint probability distributions of generated photon pairs. Parts (a) and (b) show the joint position and momentum distributions when pumped with a laser (red), parts (c) and (d) show the respective distributions when pumped with an LED (blue). Horizontal axes denote the position or momentum of the signal; vertical axes denote the position or momentum of the idler. The joint distributions show the number of coincidence counts accumulated in 1 min for the laser (a, b) and in 15 min for the LED (c, d). The pairs are strongly correlated in position when pumped with either the laser or the LED, while strong anti-correlation of their momenta occurs only for a transverse coherent pump beam. The black areas depict parts that have not been measured, since nearly no counts were expected.

In the paraxial approximation, $\Delta\kappa$ scales as the square of the difference in the transverse momenta $p_s - p_i$, as can be seen from a Taylor expansion of $\kappa_j = \left(k_j^2 - p_j^2/\hbar^2\right)^{1/2}$ for $p_j \ll \hbar k_j$, where k_j is the modulus of the wave vector of the respective field [28]. With the help of a rotated

Optics EXPRESS

coordinate system $p_\pm \equiv (p_s \pm p_i)/\sqrt{2}$, we can rewrite the angular intensity profile to $P_\mathcal{E} = P_\mathcal{E}(p_+)$ as well as the phase-matching function $P_\chi = P_\chi(p_-)$ such that they are only functions p_+ and p_-, respectively. After transforming to position space with a Fourier transformation and after an analogue rotation of the coordinates system $x_\pm \equiv (x_s \pm x_i)/\sqrt{2}$, we find a similar structure $\mathcal{P}(x_s, x_i) = \mathcal{P}_\mathcal{E}(x_+)\mathcal{P}_\chi(x_-)$. Here, the function $\mathcal{P}_\mathcal{E}(x_+)$ along the diagonal of (x_s, x_i)-space corresponds to the intensity profile of the laser and the function $\mathcal{P}_\chi(x_-)$ along the anti-diagonal is connected to the phase-matching function through a Fourier transformation. The dependence of the probability distributions on the phase-matching function as well as the pump profile and their shapes are visualized by theoretical plots in Ref. [28].

The measurements of the joint probability distributions for position space $\mathcal{P}(x_s, x_i)$ and momentum space $P(p_s, p_i)$ for both the laser and the LED are illustrated in Fig. 3. The distributions for a laser pump are shown in Fig. 3(a,b). We observe narrow ellipses along the diagonal in position space ($\Delta x_-/\Delta x_+ = 0.153 \pm 0.003$) and along the anti-diagonal in momentum space ($\Delta p_+/\Delta p_- = 0.083 \pm 0.004$), which underlines the high degree of position correlation and momentum anti-correlation. The combination of the two is a signature of entanglement and these measurements underline our heuristic arguments of a common birth zone and momentum conservation.

The joint position distribution for the LED pump is shown in Fig. 3(c). Since we designed the experiment such that the width of the intensity distribution of the LED light in the crystal is comparable to that of the laser, the two distributions are very similar. We observe a narrow ellipse along the diagonal in position space, i. e. the photon pairs are strongly correlated in position ($\Delta x_-/\Delta x_+ = 0.174 \pm 0.003$). In contrast, the joint momentum distribution for the LED shown in Fig. 3(d) demonstrates that the two momenta are *uncorrelated* ($\Delta p_+/\Delta p_- = 1.0 \pm 0.1$). Because entanglement requires a strong degree of correlation in both positions *and* momenta, we observe no position-momentum entanglement of photon pairs generated by the LED. The anti-correlations vanish not because transverse momentum conservation becomes invalid, but because the angular profile of a transverse incoherent beam is dramatically different from that of a coherent beam.

5. Pseudo-thermal light

We complete our study by experimentally investigating the effect of the coherence length l_c of a partially coherent beam on the entanglement. We spatially modulate the laser to generate a pseudo-thermal field that can be described by a Gaussian Schell-model beam [32]. Such a pump beam with a beam waist w, a radius of curvature R, and a wave number k_p leads to the variance [28]

$$\Delta p_+^2 = \hbar^2/(8w^2) + \hbar^2 w^2 k_p^2/(2R^2) + \hbar^2/(2l_c^2) \tag{4}$$

of the angular profile. The coherence length l_c causes a spread similar to the one caused by a finite radius of curvature R. We tune the coherence length [29] through the modulation strength of different random phases imprinted on the pump laser and averaged over 300 patterns. The measured uncertainties Δx_-^2 and Δp_+^2 are shown in Fig. 4(a). The position correlation remains unchanged and is independent of the coherence length [28]. In contrast, the uncertainty Δp_+^2 scales quadratically with the parameter w/l_c, following Eq. (4). The product $\Delta x_-^2 \Delta p_+^2$ shown in Fig. 4(b) highlights the impact of l_c on entanglement. For sufficiently large coherence (small w/l_c), the product is below the bound of $\hbar^2/4$. For a decreasing coherence length (increasing w/l_c), we exceed this bound and cannot verify entanglement. The laser result from Eq. (2) is consistent with the limit of a fully coherent beam. The result for the LED from Eq. (3) is far beyond what we observed for pseudo-thermal light. Although an extrapolation from our data would lead to a rough estimate of 12 µm for the coherence length of the LED, we emphasize that the Gaussian Schell model does not describe such a source very well. We believe that the uncertainty Δp_+ of the LED is not determined solely by the inverse of l_c, but is in addition limited

Optics EXPRESS

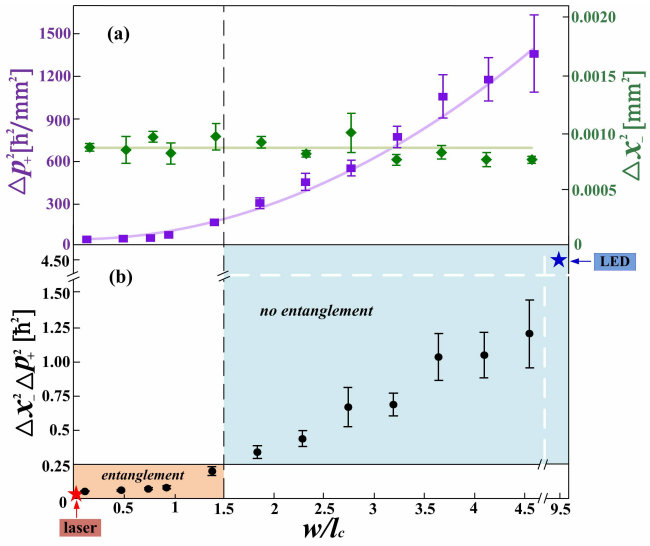

Fig. 4. Momentum anti-correlation, position correlation, and the entanglement criterion for pseudo-thermal pump beams with different coherence lengths. Part (a) shows that Δx_-^2 (green) is independent of the coherence length, whereas Δp_+^2 (purple) follows Eq. (4), as highlighted by the fit. The product $\Delta x_-^2 \Delta p_+^2$ in part (b) increases for decreasing coherence and therefore makes a transition from entangled to classically correlated photon pairs. The red star represents this product for the (coherent) laser and the blue star represents this product for the (incoherent) LED whose coherence length has been extrapolated from a fit.

by the finite aperture of the microscope lens, the low pump efficiency and the non-paraxiality of the incoherent light. An indication of similar effects might be the small difference of Δp_- between the laser and LED measurements, which could be caused by the strong focusing of the LED inside the crystal and its small longitudinal coherence [21, 33].

6. Conclusion

In in this article, we have studied the importance of spatial coherence of the pump to generate position-momentum entangled photons and demonstrated the ability to control the degree of entanglement by tuning the coherence of the pump. Since partially coherent beams have been shown to be less susceptible to atmospheric turbulence [34], our configuration might be useful for future long-distance quantum experiments and could offer a testbed for entanglement purification and distillation protocols [35]. We have further demonstrated that only for idealized situations, i.e. a perfectly coherent pump, the heuristic arguments to explain position-momentum entanglement remain valid, and we have shed light on important subtleties of the underlying phenomena of entanglement. Our results underline the relevance of the coherence of the driving force for the generation of entanglement, not only in quantum optics but also in other physical systems such as matter waves or Bose-Einstein condensates. Even though we have shown the relevance of spatial coherence for spatial entanglement, other degrees of freedom should not be affected by this property and in principle a spatially incoherent pump like sunlight could be used to generate polarization entangled photon pairs.

Funding

Canada First Research Excellence Fund award on Transformative Quantum Technologies (CFREF); China Scholarship Council (CSC) (201706310083); Fundamental Research Funds

Optics EXPRESS

for the Central Universities at Xiamen University (20720190054, 20720190057); New Century Excellent Talents in University of China (NCET) (13-0495); National Natural Science Foundation of China (NSFC) (91636109); Natural Science Foundation of Fujian Province of China for Distinguished Young Scientists (2015J06002); Natural Sciences and Engineering Council of Canada (NSERC)

Acknowledgments

We thank Armin Hochrainer for stimulating discussions. During the preparation of the manuscript, we became aware of the related work presented in Ref. [36].

Disclosures

The authors declare that there are no conflicts of interest related to this article.

References

1. A. Einstein, B. Podolsky, and N. Rosen, "Can Quantum-Mechanical Description of Physical Reality Be Considered Complete?" Phys. Rev. **47**, 777–780 (1935).
2. M. D. Reid, P. D. Drummond, W. P. Bowen, E. G. Cavalcanti, P. K. Lam, H. A. Bachor, U. L. Andersen, and G. Leuchs, "Colloquium: The Einstein-Podolsky-Rosen paradox: From concepts to applications," Rev. Mod. Phys. **81**, 1727–1751 (2009).
3. F. Flamini, N. Spagnolo, and F. Sciarrino, "Photonic quantum information processing: a review," Rep. Prog. Phys. **82**, 016001 (2018).
4. L. K. Shalm, E. Meyer-Scott, B. G. Christensen, P. Bierhorst, M. A. Wayne, M. J. Stevens, T. Gerrits, S. Glancy, D. R. Hamel, M. S. Allman, K. J. Coakley, S. D. Dyer, C. Hodge, A. E. Lita, V. B. Verma, C. Lambrocco, E. Tortorici, A. L. Migdall, Y. Zhang, D. R. Kumor, W. H. Farr, F. Marsili, M. D. Shaw, J. A. Stern, C. Abellán, W. Amaya, V. Pruneri, T. Jennewein, M. W. Mitchell, P. G. Kwiat, J. C. Bienfang, R. P. Mirin, E. Knill, and S. W. Nam, "Strong Loophole-Free Test of Local Realism," Phys. Rev. Lett. **115**, 250402 (2015).
5. M. Giustina, M. A. M. Versteegh, S. Wengerowsky, J. Handsteiner, A. Hochrainer, K. Phelan, F. Steinlechner, J. Kofler, J.-A. Larsson, C. Abellán, W. Amaya, V. Pruneri, M. W. Mitchell, J. Beyer, T. Gerrits, A. E. Lita, L. K. Shalm, S. W. Nam, T. Scheidl, R. Ursin, B. Wittmann, and A. Zeilinger, "Significant-Loophole-Free Test of Bell's Theorem with Entangled Photons," Phys. Rev. Lett. **115**, 250401 (2015).
6. S. J. Freedman and J. F. Clauser, "Experimental Test of Local Hidden-Variable Theories," Phys. Rev. Lett. **28**, 938–941 (1972).
7. J. D. Franson, "Bell inequality for position and time," Phys. Rev. Lett. **62**, 2205–2208 (1989).
8. P. G. Kwiat, A. M. Steinberg, and R. Y. Chiao, "High-visibility interference in a Bell-inequality experiment for energy and time," Phys. Rev. A **47**, R2472–R2475 (1993).
9. J.-P. W. MacLean, J. M. Donohue, and K. J. Resch, "Direct Characterization of Ultrafast Energy-Time Entangled Photon Pairs," Phys. Rev. Lett. **120**, 053601 (2018).
10. J. C. Howell, R. S. Bennink, S. J. Bentley, and R. W. Boyd, "Realization of the Einstein-Podolsky-Rosen Paradox Using Momentum- and Position-Entangled Photons from Spontaneous Parametric Down Conversion," Phys. Rev. Lett. **92**, 210403 (2004).
11. A. Mair, A. Vaziri, G. Weihs, and A. Zeilinger, "Entanglement of the orbital angular momentum states of photons," Nature **412**, 313–316 (2001).
12. J. Leach, B. Jack, J. Romero, A. K. Jha, A. M. Yao, S. Franke-Arnold, D. G. Ireland, R. W. Boyd, S. M. Barnett, and M. J. Padgett, "Quantum Correlations in Optical Angle–Orbital Angular Momentum Variables," Science **329**, 662–665 (2010).
13. M. Krenn, M. Huber, R. Fickler, R. Lapkiewicz, S. Ramelow, and A. Zeilinger, "Generation and confirmation of a (100 × 100)-dimensional entangled quantum system," Proc. Natl. Acad. Sci. U. S. A. **111**, 6243–6247 (2014).
14. Z. Xie, T. Zhong, S. Shrestha, X. Xu, J. Liang, Y.-X. Gong, J. C. Bienfang, A. Restelli, J. H. Shapiro, F. N. C. Wong, and C. Wei Wong, "Harnessing high-dimensional hyperentanglement through a biphoton frequency comb," Nat. Photonics **9**, 536 (2015).
15. J. Wang, S. Paesani, Y. Ding, R. Santagati, P. Skrzypczyk, A. Salavrakos, J. Tura, R. Augusiak, L. Mančinska, D. Bacco, D. Bonneau, J. W. Silverstone, Q. Gong, A. Acín, K. Rottwitt, L. K. Oxenløwe, J. L. O'Brien, A. Laing, and M. G. Thompson, "Multidimensional quantum entanglement with large-scale integrated optics," Science **360**, 285–291 (2018).
16. M. Erhard, R. Fickler, M. Krenn, and A. Zeilinger, "Twisted photons: new quantum perspectives in high dimensions," Light. Sci. Appl. **7**, 17146 (2018).
17. M. D'Angelo, Y.-H. Kim, S. P. Kulik, and Y. Shih, "Identifying Entanglement Using Quantum Ghost Interference and Imaging," Phys. Rev. Lett. **92**, 233601 (2004).

Optics EXPRESS

18. J. Schneeloch and J. C. Howell, "Introduction to the transverse spatial correlations in spontaneous parametric down-conversion through the biphoton birth zone," J. Opt. **18**, 053501 (2016).
19. C. H. Monken, P. H. S. Ribeiro, and S. Pádua, "Transfer of angular spectrum and image formation in spontaneous parametric down-conversion," Phys. Rev. A **57**, 3123–3126 (1998).
20. C. K. Law and J. H. Eberly, "Analysis and Interpretation of High Transverse Entanglement in Optical Parametric Down Conversion," Phys. Rev. Lett. **92**, 127903 (2004).
21. K. W. Chan, J. P. Torres, and J. H. Eberly, "Transverse entanglement migration in Hilbert space," Phys. Rev. A **75**, 050101 (2007).
22. R. M. Gomes, A. Salles, F. Toscano, P. H. S. Ribeiro, and S. P. Walborn, "Observation of a Nonlocal Optical Vortex," Phys. Rev. Lett. **103**, 033602 (2009).
23. S. P. Walborn, C. H. Monken, S. Pádua, and P. H. S. Ribeiro, "Spatial correlations in parametric down-conversion," Phys. Rep. **495**, 87 – 139 (2010).
24. A. V. Burlakov, M. V. Chekhova, O. A. Karabutova, and S. P. Kulik, "Biphoton interference with a multimode pump," Phys. Rev. A **63**, 053801 (2001).
25. A. K. Jha, M. N. O'Sullivan, K. W. C. Chan, and R. W. Boyd, "Temporal coherence and indistinguishability in two-photon interference effects," Phys. Rev. A **77**, 021801 (2008).
26. G. Kulkarni, P. Kumar, and A. K. Jha, "Transfer of temporal coherence in parametric down-conversion," J. Opt. Soc. Am. B **34**, 1637–1643 (2017).
27. A. K. Jha and R. W. Boyd, "Spatial two-photon coherence of the entangled field produced by down-conversion using a partially spatially coherent pump beam," Phys. Rev. A **81**, 013828 (2010).
28. E. Giese, R. Fickler, W. Zhang, L. Chen, and R. W. Boyd, "Influence of pump coherence on the quantum properties of spontaneous parametric down-conversion," Phys. Scr. **93**, 084001 (2018).
29. T. Shirai, O. Korotkova, and E. Wolf, "A method of generating electromagnetic Gaussian Schell-model beams," J. Opt. A: Pure Appl. Opt. **7**, 232 (2005).
30. G. Tamošauskas, J. Galinis, A. Dubietis, and A. Piskarskas, "Observation of spontaneous parametric down-conversion excited by high brightness blue LED," Opt. Express **18**, 4310–4315 (2010).
31. J. Galinis, M. Karpiński, G. Tamošauskas, K. Dobek, and A. Piskarskas, "Photon coincidences in spontaneous parametric down-converted radiation excited by a blue LED in bulk $LiIO_3$ crystal," Opt. Express **19**, 10351–10358 (2011).
32. L. Mandel and E. Wolf, *Optical coherence and quantum optics* (Cambridge University Press, Cambridge, 1995).
33. H. Di Lorenzo Pires, F. M. G. J. Coppens, and M. P. van Exter, "Type-I spontaneous parametric down-conversion with a strongly focused pump," Phys. Rev. A **83**, 033837 (2011).
34. G. Gbur, "Partially coherent beam propagation in atmospheric turbulence [Invited]," J. Opt. Soc. Am. A **31**, 2038–2045 (2014).
35. B. Hage, A. Samblowski, J. DiGuglielmo, A. Franzen, J. Fiurášek, and R. Schnabel, "Preparation of distilled and purified continuous-variable entangled states," Nat. Phys. **4**, 915–918 (2008).
36. H. Defienne and S. Gigan, "Spatially entangled photon-pair generation using a partial spatially coherent pump beam," Phys. Rev. A **99**, 053831 (2019).